The Egyptian Journal of Remote Sensing and Space Sciences 28 (2025) 205–213

Contents lists available at ScienceDirect

The Egyptian Journal of Remote Sensing and Space Sciences

journal homepage: www.sciencedirect.com

Research Paper

Is Dynamic World a Contender in Global Land-Cover Making Race? A Swift Field Assessment from Kastamonu, Türkiye

Durmuş Ali Çelik [a,*,1], Arif Oguz Altunel [b]

[a] Forestry, Arac Vocational School, Kastamonu University, Arac, Kastamonu, Türkiye
[b] Forest Engineering, Faculty of Forestry, Kastamonu University, Kastamonu, Türkiye

ARTICLE INFO

Keywords:
Sentinel-1 & 2 derivatives
Accuracy assessment
Random point
Error matrix
Kappa

ABSTRACT

Alterations in land-cover significantly influence global climate fluctuations. To utilize land resources rationally and sustainably, it is essential to identify the open-source remote sensing capabilities, the resulting products, and assess their geographical accuracies. This study conceptualized over Kastamonu province in northwestern Türkiye, focused on comparing three of the high-resolution (10 m) land-cover products; Environmental Systems Research Institute (ESRI) 2022, European Space Agency (ESA) World-Cover 2021 and Google-The World Resources Institute, Dynamic Word (DW) 2022, and 2022 Google Earth imagery were utilized for spatial comparisons. The overall accuracy (OA) and Kappa coefficient were computed, along with additional accuracy assessment metrics. OAs of land-cover maps (local accuracy), from highest to lowest, were ESRI2022; 76 %, ESA2021; 75.8 % and DW2022; 73.4 %. The Kappa coefficients for the three land-cover maps were calculated as 0.703 (very good) for ESA2021 and 0.69 and 0.68 (very good) for ESRI2022 and DW2022, respectively. The maximum user accuracy value was recorded at 92.23 % for the crops and 92.21 % for the built area classes in ESA2021. A comparison was also conducted among the corresponding class definitions. The most exemplary portrayal was observed in the categories of water, trees, and crops. Consequently, ESRI, ESA, and DW datasets were found to be fairly comparable to one another and can serve as auxiliary data in research pertaining to water, forestry and cultivated land resources.

1. Introduction

Global land-cover maps are crucial for comprehending human-land interactions through time, evaluating climate change effects, managing ecosystems sustainably, forecasting climatic trends, monitoring deforestation and conserving biodiversity (Phiri et al., 2020; Venter et al., 2022; Liu et al., 2021). The emergence of contemporary mapping technology has enabled the creation and evaluation of global databases (Altunel et al., 2020). Initially, land-cover maps were predominantly composed of manually crafted images that focused on certain local or regional areas, and they were largely devised for agricultural and cadastral objectives (Kanianska et al., 2014). The advancements of aerial photography and remote sensing technology in the mid-20th century resulted in enhanced accuracy and detail in cartography (Xiao et al., 2021; Chang et al., 2022). Thus, remote sensing technologies, including digital technology, computerized satellite image analysis, and sophisticated classification algorithms, have gained prominence in land-cover mapping (Gobbi et al., 2019). Therefore, global datasets have been created through multinational research efforts.

The spatial resolution of satellite sensors on the Moderate Resolution Imaging Spectroradiometer (MODIS; 250–500 m), PROBA-V (100 m), and Landsat (30 m) has consistently aligned with the creation of land-cover maps during the past two decades (Fahmy et al., 2023). The most prominent global land use and land-cover (LULC) maps include the National Aeronautics and Space Administration (NASA) MCD12Q1 dataset with a 500 m resolution (2001–2018) by Sulla-Menashe et al., (2019), the European Space Agency (ESA) Copernicus Global Land Service (CGLS) Land-cover dataset with a 100 m resolution (2015–2019) by Buchhorn et al., (2020), and the GlobLand30 dataset (2010) with a 30 m resolution by Chen et al., (2015). Beginning in 2014 with Sentinel-1 Synthetic Aperture Radar (SAR) and subsequently with the dual Sentinel-2 optical satellites, the European Space Agency (ESA) and the Copernicus Program commenced data collection, leading to the advancements in land-cover map making (Phiri et al., 2020). The

* Corresponding author.
E-mail addresses: dcelik@kastamonu.edu.tr (D.A. Çelik), aoaltunel@kastamonu.edu.tr (A.O. Altunel).
[1] ORCID # 0000-0002-8568-4303.

https://doi.org/10.1016/j.ejrs.2025.04.002
Received 7 January 2025; Received in revised form 20 February 2025; Accepted 6 April 2025
Available online 16 April 2025

deployment of Sentinel satellites has enabled extensive mapping of LULC studies at large scales, owing to their 10 m spatial resolution. This has been facilitated by the incorporation of state-of-the-art machine learning algorithms and the deployment of sophisticated platforms like Google Earth Engine (GEE) and several cloud computing services (Nativi et al., 2017; Zafar et al., 2024). Since 2021, three 10 m LULC maps derived through Sentinel-2 imageries have been available in worldwide scale. These comprise of Google's Dynamic World (DW) (Brown et al., 2022), ESA World-Cover (ESA) (Zanaga et al., 2021), and Esri (ESRI) (Karra et al., 2021; Altunel and Çelik, 2025).

All three products receive periodic upgrades while ESA and ESRI get annually updated, whereas the LULC maps are produced nearly in real-time, utilizing images acquired in every five days for DW. ESRI and DW were developed via deep learning models trained over a reference dataset. This dataset had over 5 billion Sentinel-2 pixel patches that were manually annotated. The dataset was derived from 24,000 image blocks, each measuring 510 × 510 m grid, and these blocks were collected from various locations worldwide (Brown et al., 2022). Conversely, ESAWC is produced through the utilization of a random forest algorithm technique that has been trained on manually labeled pixels inside 100 × 100 m grids over 141,000 distinct worldwide sites (Zanaga et al., 2021).

In light of the significance of global land-use and land-cover (LULC) maps for diverse purposes and the substantial variations in the creation of each 10-meter final product, our objective was formulated to see how the same satellite imagery, although ESA benefited from Sentinel-1 as well, would be methodologically altered to produce a different product and how their spatial compatibility and regional accuracies would compare against a visually rectified diverse landscape hand-picked in Kastamonu, Türkiye. In order to assess precision at a regional level, we utilized a vector dataset derived from manually digitized Google Earth imagery as a validation dataset. We further substantiated this claim by utilizing a polygon-based regional reference dataset (stand map) that is officially employed in forest management practices across Türkiye and examined the variations in spatial alignment and accuracy across different land-use and land-cover (LULC) classes, and discussed the main drawbacks and advantages of the three datasets.

2. Material and methods

2.1. Study area

Türkiye possesses significant biodiversity owing to its geographical position, climatic diversity (Euro-Siberian, Mediterranean, Iran-Turanian) and the presence of various habitats. Encircled by major seas on three sides, the terrain has a difficult topography, descending and ascending to low elevations in the west and high elevations in the east. The study area is situated between the longitudes of 33°43′ and 33°48′ E, and the latitudes of 41°18′ and 41°22′ N, spanning an area of 6957 ha in Kastamonu province, Türkiye (Fig. 1). The primary rationale for selecting this area for the study is the appropriateness of the comparative land categorization data presence against the diversity of classes presented in DW, ESA and ESRI datasets.

2.2. Validation

Here, manual digitizing is made from satellite imagery provided by Google Earth, a method that provides high accuracy and flexibility. However, it has limitations such as time and labor intensity, subjectivity, and scalability issues, thus further rectification was applied in ArcGIS 10.8 to harmonize the border consistencies. In addition, the forest management stand map, which is a polygon-based regional reference dataset in practical use in forest management practices across Türkiye supported our validation dataset making effort. While digitizing the validation classes, Trees, Crops, Water, Grass, Rangeland, Build-area, and Bare-ground classes were meticulously devised and materialized. Automated methods are advantageous in terms of speed and scalability, but they have difficulties such as accuracy and training data requirement. The ideal approach would be to combine these two methods: manual digitization can be used as reference data for automatic methods, or the results of automatic methods can be corrected manually. In this way, both accuracy and efficiency can be achieved. Although available, machine-learning algorithms using the same set of temporally suitable data were not preferred because they would certainly have produced or resembled to one or more of the same map/dataset results that we had already acquired and compared. Having the ultimate precision was only possible through manual intervention.

2.3. Data and Preprocessing

Three prominent datasets that offer global land-cover information were utilized, alongside the land-cover of the study area for comparison. The achievement of 10 m terrestrial resolution, owing to the success of Sentinel-2 mission, in all datasets presented a significant opportunity to demonstrate the rapid and extensive advancement in global data. The initial and more known dataset was the 10 m global map for ESRI (2022), released by ESRI in June 2023. The second dataset was another global map (ESA) with the identical resolution of 10 m for 2021, published by the European Space Agency in October 2022. The third dataset, which was released as the product of Google's Earth Engine and Google Cloud AI Platform, developed and made available for use in 2022, was "DW" (Table 1).

2.3.1. ESRI dataset

Since 2017, ESRI has been generating high-resolution, precise and comparable global maps (LULC) in a time series format. ESA Sentinel-2 mission's six bands of surface reflectance data; 10 m visible blue, green, red, near infrared, and two 20 m shortwave infrared bands were utilized to construct them. Annually, high-resolution LULC were generated utilizing Impact Observatory's deep learning AI terrain classification model developed by the National Geographic Society, and billions of human-tagged image pixels were used to train the model. The algorithm generates LULC estimations for nine classes: Water, Trees, Flooded Vegetation, Crops, Built Area, Bare Ground, Snow/Ice, Clouds, and Rangeland (URL-1, 2025). The model synthesizes various images collected over the year in question to produce a definitive map for the year in question (Karra et al., 2021). The precision of ESRI estimations differed by land-cover categories. The overall accuracy of these datasets looked often rather satisfactory; however, it could fluctuate considerably among various land-cover classes due to topographical complexity and the quality of the input data utilized for classification.

2.3.2. ESA dataset

Regional or continental land-cover maps were produced using coarse-resolution satellite imageries (>100 m) up until the turn of 21th century. First Landsat, then Sentinel-2 global depositories started showing signs of maturing with reasonably high resolution imageries, so new datasets started emerging relatively quickly. Motivated by the 2017 World-Cover conference, ESA initiated the World-Cover project. The primary deliverable of this project, which consisted of 11 land-cover classes (tree, shrub-land, grassland, cropland, built-up land, bare/sparse vegetation, snow and ice, water, herbaceous wetland, mangroves, moss and lichen) made available as a freely accessible global land-cover dataset at a resolution of 10 m. This dataset, which was the culmination of both Sentinel-1 (SAR) and Sentinel-2 imageries, appeared to have an edge over the others (Liu et al., 2024), was visually assessed for spatial correctness and ambiguity in map comparisons, utilizing two datasets including over 200,000 reference data points .(ESA, 2020; URL-2, 2025)

2.3.3. Dynamic World dataset

Since 2021, Dynamic World data, developed by Google and the World Resources Institute, has offered global land-use and land-cover

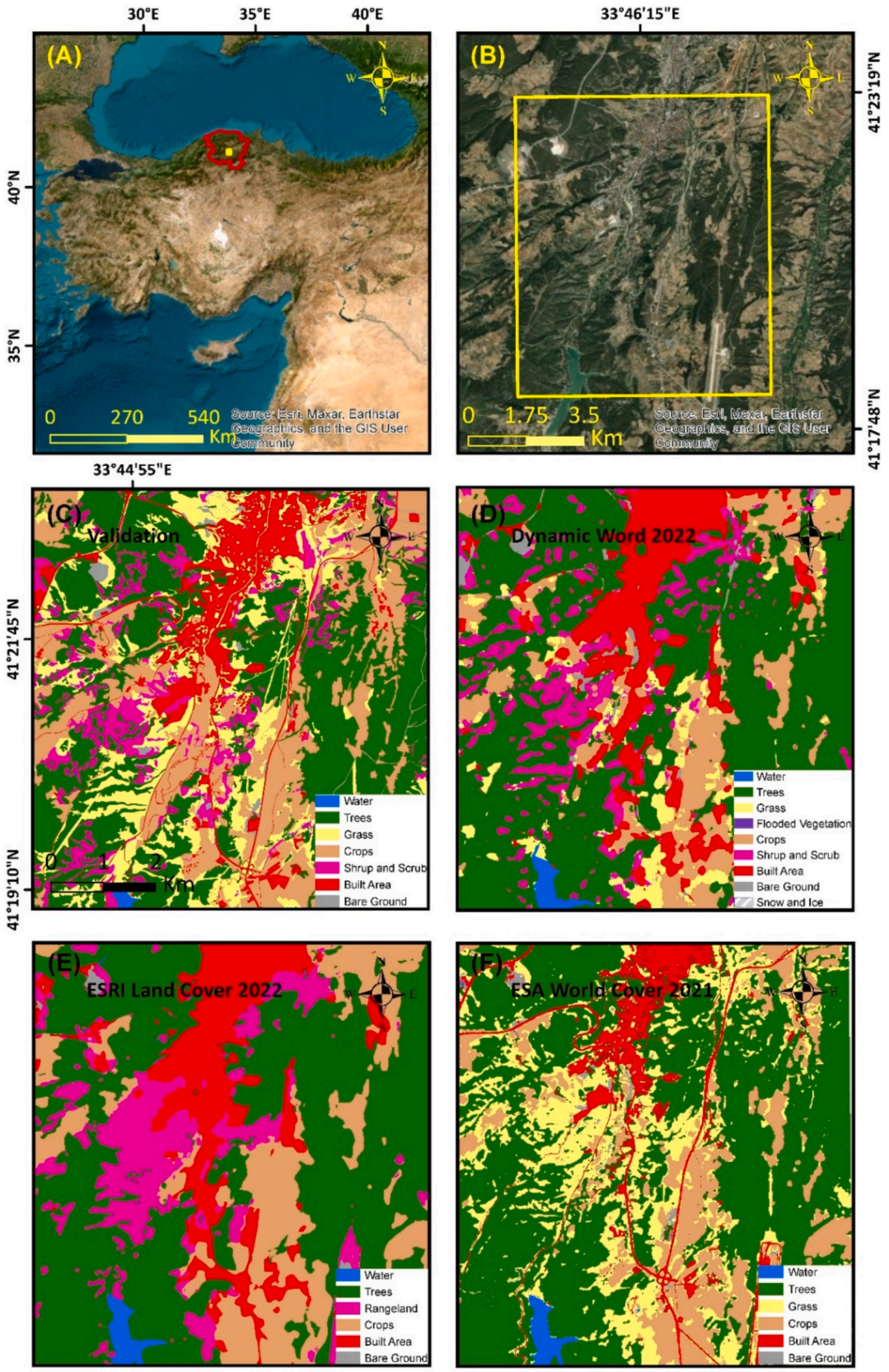

Fig. 1. Turkish extent of the study area (A), Present day study area (B), Validation (C) DW (D) equivalent, ESA (E) and ESRI (F).

Table 1
General characteristics of global land-cover datasets used in the study area.

	DW (2022)	ESRI (2022)	ESA (2021)
Producer	Google ve World Resources Institute	Environmental Systems Research Institute	The European Space Agency
Resolution	10 m	10 m	10 m
Remote sensing image	Sentinel-2	Sentinel-2	Sentinel-1-2
Production method	Fully Convolutional Neural Network	A machine learning and A Deep learning	A machine learning approach, specifically Random Forest classification
Overall global accuracy	77.8 %, Brown et al., 2022	86 %, Karra et al., 2021 75 % Venter et al., 2022	75–76 %, Zanaga et al., 2021
Datasets acronyms	DW-2022	ESRI-2020	ESA-2020
Validated Download link	https://code.earthengine.google.com/88968b814f31b0c49698ca5e28068b52	https://livingatlas.arcgis.com/landcoverexplorer/#mapCenter=-66.80083%2C-9.32196%2C11&mode=step&timeExtent=2017%2C2023&year=2022	https://worldcover2021.esa.int/downloader

maps at a spatial resolution of 10 m through GEE at no cost, utilizing Sentinel-2 imageries, machine learning algorithms, and cloud computing platforms (Brown et al., 2022; Venter et al., 2022). The Fully Convolutional Neural Network approach was employed to classify DW data. Due to the employed model, the imageries were annotated for nine categories: water, trees, grass, flooded vegetation, crops, shrub and scrub, built area, bare land, and snow and ice. Sentinel-2 imagery was employed for classification, excluding the Coastal and Aerosol (B1), Visible and Near Infrared (B8A), Water Vapor (B9), and Shortwave Infrared (B10) bands (Brown et al., 2022).

2.4. Methodology

Study comprised of two approaches;

1. Among comparison of global land-cover providers: DW, ESA and ESRI,
2. Accuracy assessment of each dataset with a comparable field verified dataset.

The classification of land-use/cover and the accuracy assessment in the study area were conducted utilizing the technique illustrated in Fig. 2. During the accuracy evaluations, the grass class, absent from the Esri2022, was incorporated into the Rangeland class; hence, the grass class in the validation data was also categorized under either the Shrub & Scrub or Rangeland class. The Mangroves, and Moss and Lichen classes in the ESA2022 map were excluded from evaluation as they were absent in our study area.

2.4.1. Random point generation and accuracy assessment

The accuracy assessment of the ESRI2022, ESA2021, and DW2022 maps utilized in the study region was conducted by generating an accuracy evaluation point layer by the simple random sampling (SRS) method, employing spatial processing capabilities in ArcGIS 10.8. 500 distinct sampling points were assigned for each dataset. The attribute table for this layer comprised of three fields: "FID" (identifier), "Classified" (the value of the classified land-cover at the specified location), and "GrndTruth" (Ground truth). Upon gathering the reference data for each class, the actual land-cover ground value for each point was incorporated from the high-resolution satellite imagery corresponding to the reference data of each class. The accuracy evaluation point layer was subsequently utilized for calculating the confusion matrix (Naghibi et al., 2021). Generating user accuracy (UA) (Equation (1), producer's accuracy (PA) (Equation (2), overall accuracy (OA) (Equation (3), and Kappa statistics are typically the accepted norm in remote sensing, as comprehensive explanations provided in numerous studies (Congalton, 1991; Stehman and Foody, 2019). Landis and Koch (1977) first stated that the Kappa value varied between −1 and + 1. A kappa score of "0″ signified that the agreement between raters aligned with what would be anticipated by the random chance. A positive score signified that the concordance among raters exceeded what would be anticipated by the random chance. Kappa values ranging from 0.41 to 0.60 were deemed moderate, 0.61 to 0.80 were regarded as good, and 0.81 to 1.00 were classified as exceptional.

$$UA = \frac{\text{Number of Correctly Classified Ponit in each Category}}{\text{Total Number of Classified Point in that category (Row total)}} * 100 \quad (1)$$

$$PA = \frac{\text{Number of Correctly Classified Ponit in each Category}}{\text{Total Number of Classified Point in that category (Column total)}} * 100 \quad (2)$$

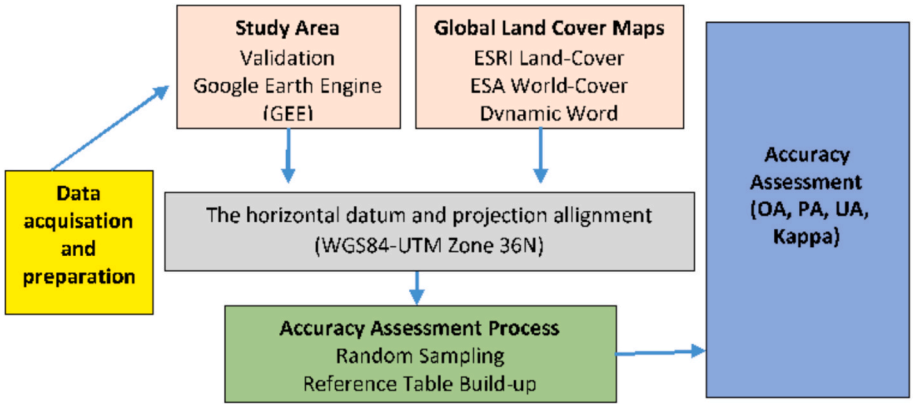

Fig. 2. Flowchart for LULC classification and accuracy assessment.

$$OA = \frac{\text{Total of Correctly Classified Ponit in each Category (diagonal)}}{\text{Total Number of Referance Point}} * 100 \quad (3)$$

3. Results

3.1. Comparison of three land-cover datasets

The outcomes of area analysis and positioning accuracy for the three datasets utilized in the study were assessed under two principal categories.

3.1.1. Spatial analysis of classes

Spatial comparisons of land-cover classifications are essential. The acreages of various land classes for three land-cover datasets in Northern Türkiye are presented in Table 2 and Fig. 3.

When compared with each other and against the validation dataset, the water class in DW, ESRI and ESA datasets, as illustrated in Table 2 and Fig. 3, exhibited similar behavior and demonstrated the same trend. The water class surface area ratio to the overall area was 0.89 % in ESA, while DW and ESRI produced 1.09 %, all aligning with the 0.93 % ratio produced in the validation dataset. The percentages of forest areas across the land-cover datasets were more or less uniform, with DW at 52.7 %, ESRI at 50.02 % and ESA at 52.73 %, but these percentages appeared somewhat excessive against the validation dataset's result of 41.03 %. The comparable arable acreage calculated in crop class at 1607.1 ha was above what were respectively calculated at DW with 1160.82 ha, at ESRI with 1385.96 ha and at ESA with 1083.98 ha.

Built Area in the validation was calculated at 556.73 ha, whereas ESA yielded the closest approximation value of 676.82 ha. Nonetheless, ESRI identified the atypically high number of acreage, totaling 1,116.76 ha, yet DW also recorded rather high 997.54 ha. When subjected to a specific class assignment ESRI and DW tended to overemphasize.

Bare Ground acreage was found at 75.42 ha in the validation while ESA again produced the closest comparison at 65.36 ha. Both ESRI and DW were at the lowest and highest ends at 37.10 (0.53 %) and 107.99 (1.55 %), respectively.

The evaluation of the Shrub and Scrub (Rangeland) class revealed that it did not register any value in ESA classification. In the validation dataset, the area was 717.9 ha, while ESRI and DW reported 861.86 ha and 578.39 ha, comparably.

Grass was formerly classified as a category in ESRI maps; however, it seemed to have been eliminated from 2022 dataset. The acreage and percentage values of the grass class in ESA and DW datasets exhibit significant discrepancies attributable to the differing algorithms. The validation dataset had an area of 1,080.55 ha, constituting 15.53 % of the total area. The nearest result was ESA at 1,400.33 ha, constituting 20.13 % of the entire area. The most distant result was DW, representing 5.20 % of the total area, which was the equivalent to 361.71 ha. The DW dataset included a Flooded Vegetation (FV) class (0.02 ha), which was absent in both ESA, ESRI, and validation datasets, thus no comparison was performed on this class. The 'Mangroves' and 'Moss and Lichen' categories identified in ESA dataset did not exist in our study area.

3.2. Accuracy assessment

Five hundred random sample locations were assigned for each dataset. The overall accuracy (OA) and Kappa coefficients of the maps were computed. Besides, the user (UA) and producer (PA) accuracies pertaining to various classes were presented in Table 3. The findings indicated that ESRI possessed the greatest overall accuracy (OA) value at 76 %, succeeded by ESA at 75.8 % and DW at 73.4 %. Conversely, to the overall success of ESRI, the ESA, ESRI and DW maps produced meager but closely lined up Kappa values of 0.703, 0.699 and 0.68, respectively. Upon general evaluation, it was evident that the "OA" and Kappa statistics of the three land-cover maps were comparable (Table 3).

For specific class evaluations, ESRI scored fairly high percentages in Water (UA: 92.0 %, PA: 86 %), Bare ground (UA: 90.0 %, PA: 76 %), Trees (UA: 80 %, PA: 86 %) and Built area (UA: 81 %, PA: 86 %), whereas SS-RA (UA: 54 %, PA: 61 %) and Crops (UA: 77.0 %, PA: 75 %) probably resulting from the absence of a Grass class, negatively affected the overall performance of the dataset (Table 3).

Similarly, ESA excelled in Crops (UA: 92.23 %), Built area (UA: 91 %, PA: 92.21 %), Water (UA: 91.7 % PA: 84.6 %), Bare ground (UA: 80.7 %, PA: 82.1 %) and Trees (PA: 88.3 %) evaluations, while Grass (UA: 63.6 %, PA: 79 %) and Crops (PA: 74.8 %) classes were decisive in the overall and Kappa line-up (Table 3).

Although lined-up in the last place as a result of the more number of classes with less than ideal performance; Bare ground (UA: 57.1, PA: 62.8 %), Grass (UA: 70.2 %, PA: 63.5 %), SS-RA (UA: 64.6, PA: 73.7 %), Crops (UA: 79.3 %, PA: 73.4) and Built area (UA: 78.6 %, PA: 68.8 %), DW still managed a similar trend in the overall comparison with Trees (UA: 87.4 %, PA: 86.6 %) and Water (UA: 83.3.0 %, PA: 90.9 %) classes strengthening the dataset's performance.

Since Flooded vegetation and Snow and Ice classes were absent in the study area, they were left outside the accuracy evaluation.

Despite the datasets seemed similar within the class areas, their locational correctness indicated a necessity for additional local verification points during their construction. Upon examining the class boundaries of sample regions collected from various locations within the study area, discrepancies between the observed boundary delineations and the verification map boundaries were evident (Fig. 4). Among the datasets, the ESA had the most accurate spatial boundaries with more than 70 % overall accuracy. Nonetheless, inaccuracies arose from the specification of the SS-RA class in the ESA dataset. It appeared that in the production of ESRI dataset, Built areas were surrounded with an invisible buffer superficially increasing the acreage. Tree and Crop class delineations looked misplaced and linear asphalt road and lawn placements showed inaccuracies resulting from algorithmic misinterpretations. DW dataset seemed displaying the class boundaries within their designated areas, but with more lesser-performing scores and missing class definitions, it was the least favorable dataset in this study.

Table 2
The acreages calculated over validation and comparison datasets.

LC Class	Validation		DW		ESRI		ESA	
	Area (ha)	%	Area (ha)	%	Area (ha)	%	Area (ha)	%
Water(W)	65.03	0.93	76.11	1.09	75.60	1.09	61.81	0.89
Trees (T)	2,854.31	41.03	3,672.42	52.79	3,479.77	50.02	3,668.74	52.73
Grass(G)	1,080.55	15.53	361.71	5.20	–	–	1,400.33	20.13
Flooded Vegetation(FV)			0.02	0.00	–	–	–	–
Crops(C)	1,607.10	23.10	1,160.82	16.69	1,385.96	19.92	1,083.98	15.58
Shrup and Scrub (Rangeland)	717.90	10.32	578.39	8.31	861.86	12.39	–	–
Built Area(BA)	556.73	8.00	997.54	14.34	1,116.76	16.05	676.82	9.73
Bare Ground(BG)	75.42	1.08	107.99	1.55	37.10	0.53	65.36	0.53
Snow and Ice(SI)	0.00	–	2.05	0.03	–	–	–	–
Total Area (ha)	6,957.03	–	6,957.03	–	6,957.03	–	6,957.03	–

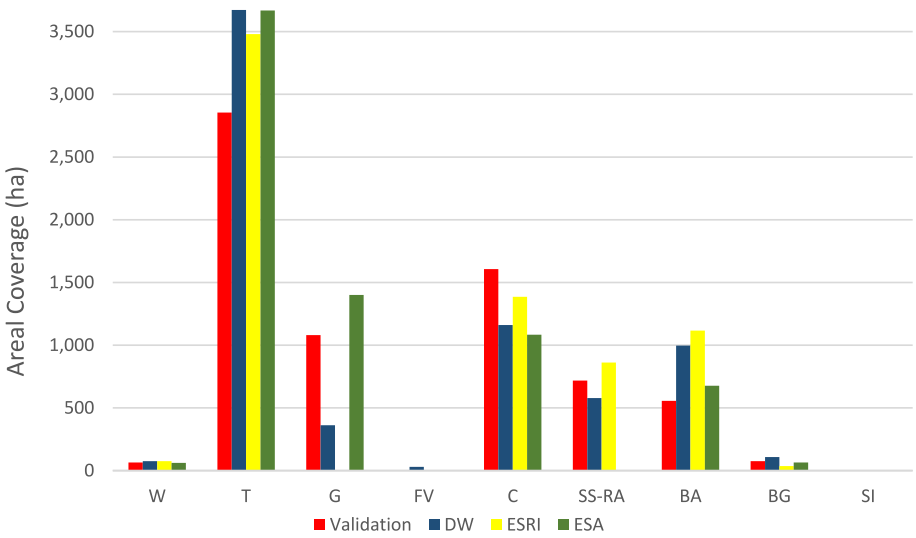

Fig. 3. Areal coverages (ha) of classes in comparison and validation datasets.

Table 3
Accuracy assessments of three datasets and the individual classes.

Datasets		Land-cover Classes										
	Accuracy Measures (%)	Water	Trees	Grass	Flooded Vegetation	Shrup and Scrub (Rangeland)	Bare Ground	Crops	Built Area	Snow and Ice	OA	Kappa
	UA	83.3	87.4	70.2	–	64.6	57.1	79.3	78.6	–	73.4	0.68
DW	**PA**	90.9	86.6	63.5	–	73.7	62.8	73.4	68.8	–		
ESRI	**UA**	92.0	80.0	–		54.0	90.0	77.0	81.0		76.0	0.69
	PA	86.0	89.0	–		61.0	76.0	75.0	86.0			
ESA	**UA**	91.7	62.9	63.6		–	80.7	92.23	91.0		75.8	0.70
	PA	84.6	88.3	79.0		–	82.1	74.8	92.21			

4. Discussion

The various procedures and strategies employed by the agencies generating land-cover datasets influenced the performance of all three tested products. Specifically, varying dataset regulations including categorization systems and methods might result in disagreements among products and impede the comparison of datasets within identical classes (Herold et al., 2008; Yang et al., 2017; Gao et al., 2020). The discrepancies in certain sub-definitions of land-cover classes within classification systems contribute to the low geographic consistency among ESA, ESRI, and DW products. The global classification systems are mostly utilized for worldwide classifications, considering the attributes of global datasets, therefore this situation necessarily influenced the specific studies and implementations in local contexts (Brown et al., 2022; Kang et al., 2022; Karra et al., 2021; Altunel and Çelik, 2025).

Although this study indicated that ESRI, ESA, and DW utilized the same data, common Sentinel-2 in all and Sentinel-1 support in ESA, as the data source for extracting surface cover categories, three classes, Shrub and Scrub (Rangeland), Built Area, and Bare Ground, exhibited low spatial consistency in all. This phenomenon was clearly apparent through the different class delineations visible in Fig. 1. The exclusion of the Shrub and Scrub (Rangeland) and Grass classes in ESA and ESRI, respectively resulted in significant discrepancies in the consistency of datasets. The strong spatial similarity among the Water, Trees, and Crops classes was attributable to their closely related class distinction definitions. The accuracy of algorithms designed for land-cover identification using surface reflection values may certainly improve if other characteristics such as vegetation cover, tree height, and density are better incorporated (Weng, 2012). Land-cover dataset must include well-articulated definitions to mitigate the ambiguity arising from the classification methods (Fitzgerald and Lees, 1994; Foody, 2002).

Our validation results indicated that the user and producer accuracies for the Water class were 92 % in ESRI and 90.9 % in DW, respectively. ESRI and DW accuracies were lower when water classification was concerned for ESA (UA: 91.7 % and PA: 84.6 %), ESRI (PA: 86 %), and DW (UA: 83.3 %) (Table 3). These findings were consistent with some studies conducted abroad. UA varied between 91 and 98 % and PA between 84.0 and 90.8 % in Water classification in ESRI products, whereas it varied between 82 % and 95 % and PA between 63.3 % and 84.6 % in ESA. In DW, on the other hand, UA varied between 69.5 % and 87.5 %, and PA varied between 87.3 % and 97.5 %. (Brown et al., 2022; Chaaban et al., 2022; Ding et al., 2022; Kang et al., 2022; Wang et al., 2023). Global and local research indicated that UA ranged around 90.29 % and accounted for 1 % of the studied extent, while PA was around 83.0 % with similar extent in water class of ESRI products (Brown et al., 2022; Chaaban et al., 2022; Ding et al., 2022; Kang et al., 2022; Dash et al., 2023). Studies observed that the water/wetland classification posed the greatest challenge for automated mapping, since the related algorithms could incorporate any surface cover type provided it is established throughout seasonal periods (Gong et al., 2019). However, the utilization of Sentinel satellites has emerged as a significant source of Synthetic Aperture Radar (SAR) data for water mass mapping. The spatial resolution provided at 10 m in frequent intervals facilitated long-term monitoring and analysis of surface water variations through the generation of time series data. Consequently, it provided that the water classification zones and delineations with rather acceptable precisions. ESRI, ESA, and DW products can further support water-related research in arid places (Brown et al., 2022; Feng, 2021; Schlund and Erasmi, 2020).

Tree class based user accuracies of the three datasets lined up as DW 87.4 %, ESRI 80 %, and ESA 62.9 %, respectively. When it came to producer accuracies, ESRI was found to be 89 %, ESA 88.3 % and DW

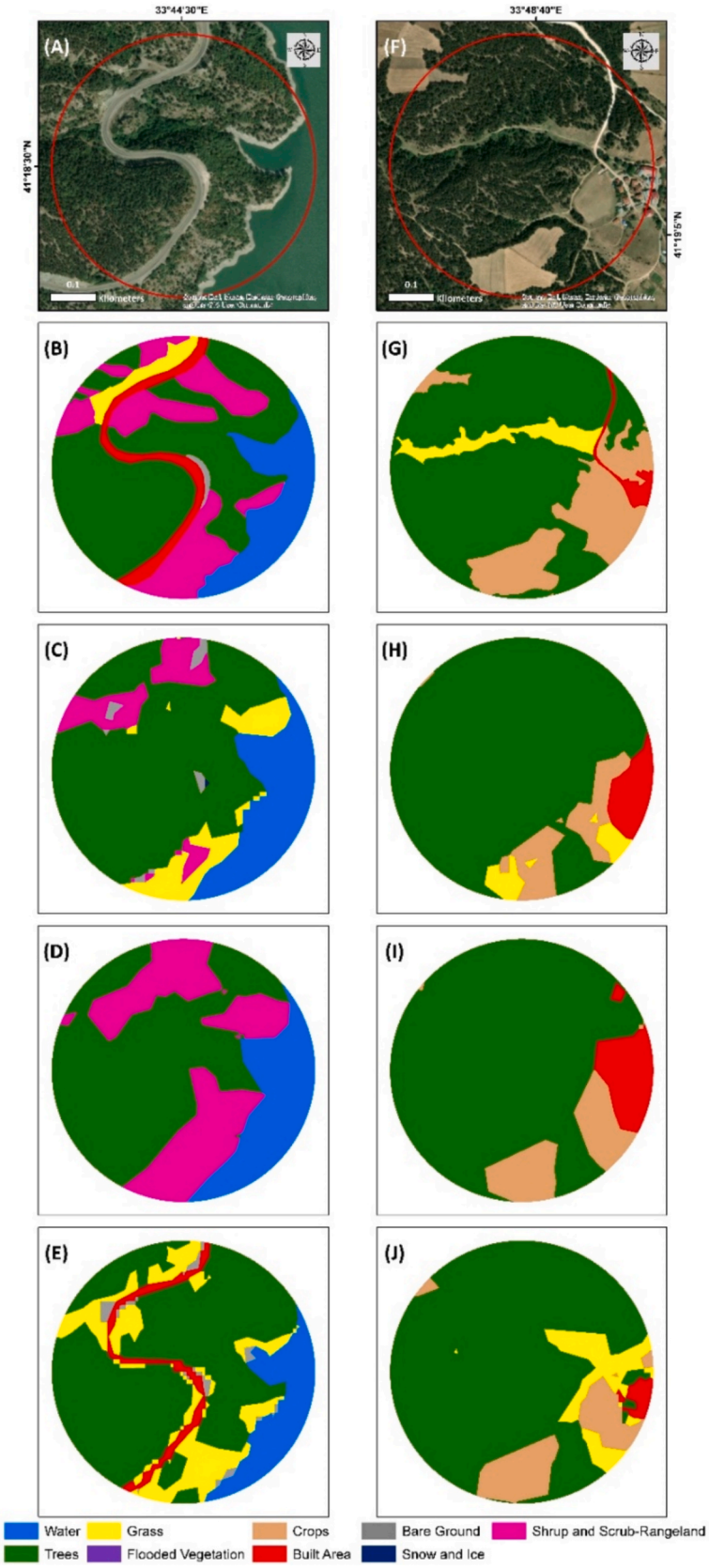

Fig. 4. High-resolution satellite image of the study area (A) from the southern part (lake and its surroundings), (F) from the eastern part (Built area and Crops); (B,G) from the validation Map-2022; example sites showing the positional accuracies of (C,H) from ESRI, (D,I) from ESA and (E) from DW datasets.

86.6 % (Table 3). Our findings were either compatible or better than various investigations conducted internationally and locally as indicated regarding the Trees class: ESRI UA ranged from 91 % to 98 % and PA from 84.5 % to 90.8 %; ESA UA ranged from 82 % to 95 % and PA from 63.3 % to 84.6 % and Dynamic World UA ranged from 69.5 % to 87.5 % while PA ranged from 87.3 % to 97.5 % (Brown et al., 2022; Chaaban et al., 2022; Ding et al., 2022; Kang et al., 2022; Wang et al., 2023). High-resolution satellite imageries remain accessible at almost everywhere. It seemed that the anticipated accuracy has not yet been attained, particularly in forested regions. The rationale for this finding is thought to be fact that the forest cover is heterogeneous, exhibiting variations among shrubs, meadows, and habitats. Thus, we anticipate that accuracies will further improve as the enhanced class delineation algorithms continue to improve.

Agricultural land is a vital resource for agricultural productivity and food supply. The state of these lands is crucial for global food security and socioeconomic stability (Han et al., 2007). The ability to determine the boundary line of agricultural land resources for all three datasets was quite sufficient (Fig. 4) so that the rather reasonable user accuracies were detected in the crops classes. UA percentages ranged from 77 % in ESRI to 79.3 % in DW and to 92.23 % in ESA, while PA values were found to be 75 % in ESRI, 74.8 % in ESA and 73.4 % in DW datasets. Depending upon some studies conducted globally or locally, UA varied between 68.75 % and 96.3 %, and PA ranged between 57 % and 89 % in crops class of ESRI products. In ESA dataset, UA varied between 68.2 % and 9 % and PA varied between 47 and 89.27 %. Finally in DW dataset, UA varied between 88.9 % and 97.1 % and PA varied between 60 % and 78.60 % (Brown et al., 2022; Chaaban, et al., 2022; Ding et al., 2022; Kang et al., 2022; Wang et al., 2023, Zhu et al., 2024). Therefore, we concluded that all three datasets could safely provide auxiliary data for research on arable land resources. DW's utilization of pixel-based probability scores may offer more efficient approaches for estimating pixel classification accuracies (Sales et al., 2021).

In this study, the overall accuracy of ESRI at 76 % reached a similar accuracy reported as global accuracy rate of 75 % by Venter et al., (2022). Comparably, the ESA Word-cover overall accuracy at 75.8 % in this study was slightly lower than what Zanaga et al., (2022) reported at 76.7 %. Although the global overall accuracy of the Dynamic World dataset was approximated at 83 % (Brown et al., 2022), we calculated it at 73.4 % in the study. SAR inclusion in the making of ESA dataset did not significantly improve its overall accuracy.

Finally, when Kappa coefficients (Landis and Koch, 1977) of three datasets were concerned, ESA was found as 0.703 (substantial), while ESRI and DW yielded as 0.69–0.68 (substantial), although Ding et al., (2022) and Zhu et al., (2024) reported the kappa coefficient of the ESA world-cover map having the values of 0.66 (good) – 0.7667 (very good), ESRI 0.69 (good) – 0.8292 (very good) and DW 0.7757 (very good).

5. Conclusion

This study assessed the accuracy assessment and comparative analysis of global high-resolution datasets' practicality for planners and decision-makers. The findings indicated the subsequent;

1. The OA of ESRI dataset was the highest at 76 %, followed by ESA at 75.8 % and DW produced the lowest at 73.4 %,
2. In the class land area consistency analysis of three land maps, the most successful land class was Water, followed by Trees and Crops. The land classes revealed that they were mostly distributed in areas with low surface heterogeneity and singular land-cover types. The main reason for the low consistency between the three products was the fact that vegetation cover, tree height, and density were different in each data while defining Shrub/Scrub (Rangeland), Grass, and Bare ground classes. Besides, Built areas seemed as surrounded with an invisible buffer, increasing their actual extents,
3. ESRI, ESA and DW datasets could be used as auxiliary data for research on Water, Trees and Crops resources. In general, Kappa (DW: 0.68, ESA: 0.70, and ESRI: 0.69) values of the three global products were low in remote sensing sense. The limit of our study appeared as being the sole comparison trial from a small part in Türkiye, which can be viewed as a shortcoming in terms of the global accuracies of these datasets. However, as more and more studies start appearing from other parts of the Earth dealing either with these or with even more of the similar datasets, their suitabilities for broader land cover types will further be validated. Sentinel program has been revolutionary in its short lifespan in remote sensing, but we do not think it would be the ultimate. There will surely come even higher resolutions and better algorithms to map more number of land-cover classes in the future. Thus, to assess the impacts of climate change on both global and regional scales in the future, it would be essential to enhance the precision of land-cover datasets to support the works on vegetation alterations, carbon sequestration, and biodiversity monitoring.

CRediT authorship contribution statement

Durmuş Ali Çelik: Writing – review & editing, Writing – original draft, Visualization, Validation, Supervision, Software, Resources, Project administration, Methodology, Investigation, Funding acquisition, Formal analysis, Data curation, Conceptualization. **Arif Oguz Altunel:** Writing – review & editing, Writing – original draft, Software, Resources, Project administration, Methodology, Investigation, Funding acquisition, Formal analysis, Data curation, Conceptualization.

Declaration of competing interest

The authors declare that they have no known competing financial interests or personal relationships that could have appeared to influence the work reported in this paper.

Acknowledgment

We thank both DW, ESRI and ESA for freely disseminating their end-products for everyone to enjoy.

Appendix A. Supplementary data

Supplementary data to this article can be found online at https://figshare.com/articles/media/GEE_Script/28754828?file=53512826.

References

Altunel, A.O., Akturk, E., Altunel, T., 2020. Examining the PALSAR-2 Global forest/non-forest maps through Turkish afforestation practices. Int. J. Remote Sens. 41 (16), 6071–6088.
Altunel, A.O., Çelik, D.A., 2025. Comparison of SAR and Optical derived Data used in Forest Cover Detection; PALSAR-FNF vs. ESRI LAND-COVER over North Central Türkiye. Int. J. Environ. Sci. Technol. 22 (5), 3641–3654.
Brown, C.F., Brumby, S.P., Guzder-Williams, B., Birch, T., Hyde, S.B., Mazzariello, J., Czerwinski, W., Pasquarella, V.J., Haertel, R., Ilyushchenko, S., et al., 2022. Dynamic world, near real-time global 10 m land use land cover mapping. Sci. Data 2022 (9), 251.
Buchhorn, M., Lesiv, M., Tsendbazar, N.-E., Herold, M., Bertels, L., Smets, B., 2020. Copernicus global land cover layers—collection 2. Remote Sens. 2020 (12), 1044.
Chaaban, F., El Khattabi, J., Darwishe, H., 2022. Accuracy assessment of ESA WorldCover 2020 and ESRI 2020 land cover maps for a Region in Syria. Journal of Geovisualization and Spatial Analysis 6 (2), 31.
Chang, S., Deng, Y., Zhang, Y., Wang, R., Qiu, J., Wang, W., Liu, D., 2022. An advanced echo separation scheme for space-time waveform-encoding SAR based on digital beamforming and blind source separation. Remote Sens. (Basel) 14 (15), 3585.
Chen, J., Chen, J., Liao, A., Cao, X., Chen, L., Chen, X., He, C., Han, G., Peng, S., Lu, M., et al., 2015. Global land cover mapping at 30 m resolution: A POK-based operational approach. ISPRS J. Photogramm. Remote Sens. 2015 (103), 7–27.
Congalton, R.G., 1991. A review of assessing the accuracy of classifications of remotely sensed data. Remote Sens. Environ. 37 (1), 35–46.

Dash, P., Sanders, S.L., Parajuli, P., Ouyang, Y., 2023. Improving the accuracy of land use and land cover classification of landsat data in an agricultural watershed. Remote Sens. (Basel) 15 (16), 4020.
Ding, Y., Yang, X., Wang, Z., Fu, D., Li, H., Meng, D., Zhang, J., 2022. A field-data-aided comparison of three 10 m land cover products in Southeast Asia. Remote Sens. (Basel) 14 (19), 5053.
ESA (2020). WorldCover Product User Manual | V 1. 0. Tech. Rep. Available through https://worldcover2020.esa.int/data/docs/WorldCover_PUM_V1.1.pdf, last accessed in 19/03/2025.
Fahmy, A.H., Abdelfatah, M.A., El-Fiky, G., 2023. Investigating land use land cover changes and their effects on land surface temperature and urban heat islands in Sharqiyah Governorate, Egypt. Egypt. J. Remote. Sens. Space Sci. 26 (2), 293–306.
Feng, Z. 2021. Research on the Evalution of Agricultural Sustainable Development in Northwest China Based on Water Resources Carrying Capacity. Unpublished Ph.D. Thesis. Xi'an University of Technology, Xi'an, China.
Fitzgerald, R.W., Lees, B.G., 1994. Assessing the Classification Accuracy of Multisource Remote Sensing Data. Remote Sens. Environ. 1994 (47), 362–368.
Foody, G.M., 2002. Status of land cover classification accuracy assessment. Remote Sens. Environ. 80 (1), 185–201.
Gao, Y., Liu, L., Zhang, X., Chen, X., Mi, J., Xie, S., 2020. Consistency analysis and accuracy assessment of three global 30-m land-cover products over the European Union using the LUCAS dataset. Remote Sens. (Basel) 12 (21), 3479.
Gobbi, S., Ciolli, M., La Porta, N., Rocchini, D., Tattoni, C., Zatelli, P., 2019. New tools for the classification and filtering of historical maps. ISPRS Int. J. Geo Inf. 8 (10), 455.
Gong, P., Liu, H., Zhang, M., Li, C., Wang, J., Huang, H., Clinton, N., Ji, L., Li, W., Bai, Y., et al., 2019. Stable classification with limited sample: Transferring a 30-m resolution sample set collected in 2015 to mapping 10-m resolution global land cover in 2017. Sci. Bull. 2019 (64), 370–373.
Han, D., Guoqing, W., Renchao, W., 2007. Land-use change and cropland loss in the Zhejiang coastal region of China. N. z. J. Agric. Res., 50, 1235–1242.
Herold, M., Mayaux, P., Woodcock, C.E., Baccini, A., Schmullius, C., 2008. Some challenges in global land cover mapping: An assessment of agreement and accuracy in existing 1 km datasets. Remote Sens. Environ. 112 (5), 2538–2556.
Kang, J., Yang, X., Wang, Z., Cheng, H., Wang, J., Tang, H., Bai, Z., 2022. Comparison of three ten meter land cover products in a Drought region: A case study in Northwestern China. Land 11 (3), 427.
Kanianska, R., Kizeková, M., Nováček, J., Zeman, M., 2014. Land-use and land-cover changes in rural areas during different political systems: A case study of Slovakia from 1782 to 2006. Land Use Policy 36, 554–566.
Karra, K., Kontgis, C., Statman-Weil, Z., Mazzariello, J.C., Mathis, M., Brumby, S.P., 2021. Global land use/land cover with sentinel 2 and deep learning. In: 2021 IEEE international geoscience and remote sensing symposium IGARSS. IEEE, pp. 4704–4707.
Landis, J.R., Koch, G.G., 1977. The measurement of observer agreement for categorical data. Biometrics 33 (1), 159–174.
Liu, D., Chang, S., Deng, Y., He, Z., Wang, F., Zhang, Z., Yu, C., 2024. A novel spaceborne SAR constellation scheduling algorithm for sea surface moving target search tasks. IEEE J. Sel. Top. Appl. Earth Obs. Remote Sens. 17, 3715–3726.
Liu, L., Zhang, X., Gao, Y., Chen, X., Shuai, X., Mi, J., 2021. Finer-Resolution Mapping of Global Land Cover: Recent Developments, Consistency Analysis, and Prospects. AASA J. Remote Sens. 2021, 5289697.
Naghibi, S.A., Hashemi, H., Pradhan, B., 2021. APG: A novel python-based ArcGIS toolbox to generate absence-datasets for geospatial studies. Geosci. Front. 12 (6), 101232.
Nativi, S., Mazzetti, P., Craglia, M.A., 2017. View-based model of data-cube to support big earth data systems interoperability. Big Earth Data 1 (1-2), 75–99.
Phiri, D., Simwanda, M., Salekin, S., Nyirenda, V.R., Murayama, Y., Ranagalage, M., 2020. Sentinel-2 data for land cover/use mapping: A review. Remote Sens. (Basel) 12 (14), 2291.
Sales, M.H., De Bruin, S., Souza, C., Herold, M., 2021. Land use and land cover area estimates from class membership probability of a random forest classification. IEEE Trans. Geosci. Remote Sens. 60, 4402711.
Schlund, M., Erasmi, S., 2020. Sentinel-1 time series data for monitoring the phenology of winter wheat. Remote Sens. Environ. 246, 111814.
Sulla-Menashe, D., Gray, J.M., Abercrombie, S.P., Friedl, M.A., 2019. Hierarchical mapping of annual global land cover 2001 to present: The MODIS Collection 6 Land Cover product. Remote Sens. Environ. 222, 183–194.
Stehman, S.V., Foody, G.M., 2019. Key issues in rigorous accuracy assessment of land-cover products. Remote Sens. Environ. 231, 111199.
URL-1. 2025. Sentinel-2 10-Meter Land Use/Land Cover, ESRI land cover. Available through https://livingatlas.arcgis.com/landcover/, last accessed in 29/03/2025.
URL-2. 2025, Meet ESA WorldCover – Global Land Cover mapping at High Spatial Resolution. Available through https://sentinel.esa.int/web/success-stories/-/meet-esa-worldcover-global-land-cover-mapping-at-high-spatial-resolution, last accessed in 30/03/2025.
Weng, Q., 2012. Remote sensing of impervious surfaces in the urban areas: Requirements, methods, and trends. Remote Sens. Environ. 117, 34–49.
Venter, Z.S., Barton, D.N., Chakraborty, T., Simensen, T., Singh, G., 2022. Global 10 m land use land cover datasets: A comparison of dynamic world, world cover and Esri Land Cover. Remote Sens. (Basel) 14 (16), 4101.
Wang, Y., Sun, Y., Cao, X., Wang, Y., Zhang, W., Cheng, X., 2023. A review of regional and Global scale Land Use/Land Cover (LULC) mapping products generated from satellite remote sensing. ISPRS J. Photogramm. Remote Sens. 206, 311–334.
Xiao, Y., Su, X., Yuan, Q., Liu, D., Shen, H., Zhang, L., 2021. Satellite video super-resolution via multiscale deformable convolution alignment and temporal grouping projection. IEEE Trans. Geosci. Remote Sens. 60, 5610819.
Yang, Y., Xiao, P., Feng, X., Li, H., 2017. Accuracy assessment of seven global land cover datasets over China. ISPRS J. Photogramm. Remote Sens. 2017 (125), 156–173.
Zanaga, D., Van De Kerchove, R., De Keersmaecker, W., Souverijns, N., Brockmann, C., Quast, R., Wevers, J., Grosu, A., Paccini, A., Vergnaud, S., .et al. (2021). ESA WorldCover 10 m 2020 V100. Available through https://doi.org/10.5281/zenodo.5571936, last accessed in 17/03/2025.
Zanaga, D., Van De Kerchove, R., Daems, D., De Keersmaecker, W., Brockmann, C., Kirches, G., ... & Arino, O. (2022). ESA WorldCover 10 m 2021 v200.Available through https://doi.org/10.5281/zenodo.7254221, last accessed in 17/03/2025.
Zafar, Z., Zubair, M., Zha, Y., Fahd, S., Nadeem, A.A., 2024. Performance assessment of machine learning algorithms for mapping of land use/land cover using remote sensing data. Egypt. J. Remote. Sens. Space Sci. 27 (2), 216–226.
Zhu, H., Yu, T., Mi, X., Yang, J., Tian, C., Liu, P., Yan, J., Meng, Y., Jiang, Z., Ma, Z., 2024. Large-scale land cover mapping framework based on prior product label generation: a case study of Cambodia. Remote Sens. 2024 (16), 2443.